JOURNAL OF MATERIALS SCIENCE 21 (1986) 3625–3632

Formation of secondary phases and microdiscs on flux-grown $HoFeO_3$ crystals

P. N. KOTRU, S. K. KACHROO
Department of Physics, University of Jammu, Jammu 180001, India
B. M. WANKLYN
Department of Physics, Clarendon Laboratory, University of Oxford, Oxford, UK

Results of optical and scanning electron microscopic and EDAX studies, carried out on structures exhibited by $HoFeO_3$ crystals grown from the $PbO-PbF_2-B_2O_3$ flux system, are reported. Aluminium and silicon are present as impurities in the crystals studied. EDAX of certain structures indicate formation of magnetoplumbite ($PbO \cdot 6Fe_2O_3$) during the flux growth of $HoFeO_3$. Crystallization of HoOF on the $HoFeO_3$ crystal surfaces is also indicated; the process taking place almost at the end of $HoFeO_3$ crystal growth. A variety of microdisc patterns on $HoFeO_3$ crystal surfaces are illustrated. Their formation is attributed to the covering process of impurity phases by the rapidly advancing growth fronts on the $HoFeO_3$ crystal surfaces. Experimental evidence in support of this is offered by exposing the impurity phase buried under the microdisc. Precipitation of the secondary phases during the flux growth of $HoFeO_3$ crystals and their influence on the latter is discussed.

1. Introduction

Impurities have a large effect on the uniformity, shape and growth of crystals. Faces which absorb the impurity selectively grow more slowly and become the dominant ones [1]. The trapped inclusions in the crystal lattice often generate additional defects in crystals [2–6].

The rare-earth orthoferrites ($RFeO_3$: R = rare-earth element) exhibit interesting magnetic properties such as spin reorientation induced by a temperature change or an applied magnetic field where the direction of the easy axis of magnetization changes from one crystal axis to another [7, 8]. It is desirable that the growth process yields a crystal with the minimum possible defects so as to be useful for any scientific study or technical application. Flux growth yields crystals with habit faces which are suitable for topographical investigation. Although the study of surface patterns of crystals is considered to yield information about situations towards the end of growth, it does offer an opportunity to view the dynamic nature of the process by enabling one to trace the changes which the crystal might have undergone in the time interval before the cessation of growth.

In our earlier communications [9, 10], it was reported that $PbO \cdot 6Fe_2O_3$ (magnetoplumbite), ErOF and $ErBO_3$ crystallize as secondary phases in the growth of $ErFeO_3$ crystals from flux. The origin of imperfections in $ErFeO_3$ has been shown to correlate with the precipitation of secondary phases and other faults during growth.

In this paper we report results obtained on flux-grown $HoFeO_3$ crystal surfaces employing optical and electron microscopy, and the energy dispersive analysis of X-rays (EDAX) for elemental analysis.

2. Experimental details

$HoFeO_3$ crystals were grown by the flux method using the composition 22.8 g Ho_2O_3, 9.8 g Fe_2O_3, 2.4 g B_2O_3, 44.6 g PbO, 64.8 g PbF_2 and 2 g PbO_2. The whole composition pressed into a 50 cm^3 platinum crucible was soaked at 1260° C for 20 h and was then allowed to cool at 2 K h^{-1} to 850° C. From 850° C to room temperature, the cooling rate was increased to 100 K h^{-1}. To separate the resulting crystals from flux, the crucible was inverted and heated to 850° C. In this process most of the flux ran off the crystals. Finally, it was again cooled at 100 K h^{-1}. Typical features on the {1 0 0} faces were studied using the metallurgical microscope Neophot-2 (CZ-Germany) and the Cambridge Stereoscan (SU-10) SEM. Qualitative elemental analysis was carried out with the help of the EDAX attachment of the SEM.

3. Results and discussion

$HoFeO_3$ crystals show microdiscs, circular, semicircular and irregular shaped patches of preferential growth, hexagonal elevations, attachment of precipitated material and overgrowths. In order that the mechanisms of formation of the microstructures exhibited by $HoFeO_3$ surfaces are understood, the structures were studied under optical and scanning electron microscopes and analysed using EDAX (including X-ray mapping and element profile analysis).

3.1. Irregular growth fronts and patch-like structures

Fig. 1 shows wavy growth fronts on the crystal surface. The edges of the growth fronts are made markedly visible by black material. The black material appears to be impurities which are non-uniformly

0022–2461/86 $03.00 + .12

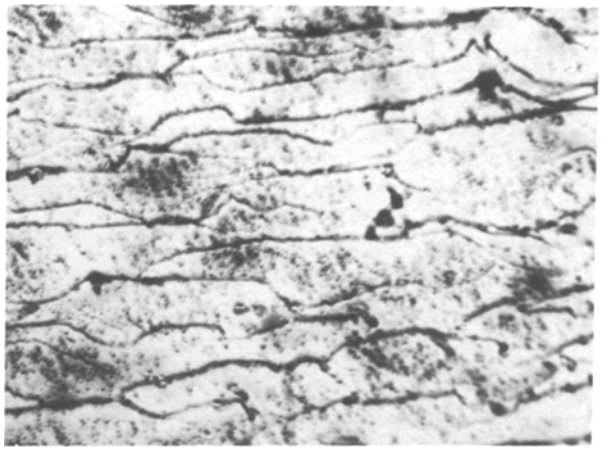

Figure 1 Wavy growth fronts on the crystal surface showing impurities along the edges of wavy growth fronts (× 400).

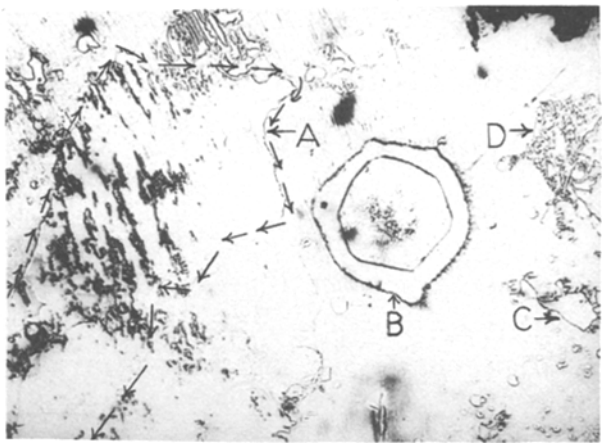

Figure 3 Different formations of irregularly shaped patches. Note precipitation of impurities along the edges of some of the patch-like formations (× 320).

precipitated along the edges of the growth fronts. The visibility of the growth fronts is considerably reduced at places where less of these impurities have been adsorbed.

One often finds impurities of this type along the boundaries or over patches of overgrowths. While these impurities appear as black particles under the optical microscope, the patches of overgrowths appear in the form of perfectly circular discs, half discs or irregular shapes. Fig. 2 illustrates all such forms of patch-like formations of overgrowths and impurities. Fig. 3 shows irregularly shaped patches (i.e. A, B, C and D, etc.). The impurities along the edges of these patches make them pronouncedly visible. In the central region of this figure we find an almost hexagonal patch staged over an almost circular (but deformed at some places – see B) patch. The black material has placed itself preferentially along the edges of these patches. It is found randomly scattered over patch A. Fig. 4 illustrates an interesting region where black material and the patch-like features co-exist. Growth lines which have independently developed are also found on the patches. A is a hexagonal overgrowth, B is a highly irregular and widely spread overgrowth (as indicated by the arrows), C is an almost circular overgrowth along with another hexagonal overgrowth over it, and D is a half microdisc (the remaining portion of which is covered by the irregular overgrowth). Evidence of independently developed growth fronts is found, as at the marked region of the circular patch (C). Some of the growth fronts on the circular patch are made prominently visible on account of precipitation of impurities along their edges. On close examination of this patch, it is clearly established that the saw-tooth appearance of the black boundary of the patch is due to poorly resolved separation of impurity particles. The impurity particles are seen to be linearly arranged along parallel rows on the central irregular patch B. The hexagonal overgrowth on the circular patch C seems to have developed over it at a later stage as is clear from the continuity of growth fronts on either sides of the hexagonal feature. The formation of these features is discussed further in the following section.

3.2. Secondary phases

In order to understand the formation of the black material and the irregular structures in the form of patches, SEM and EDAX studies were carried out.

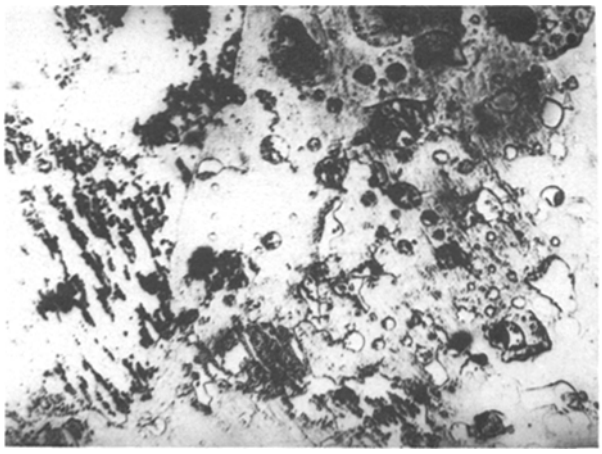

Figure 2 An optical micrograph showing patch-like formations of overgrowths and impurities (× 320).

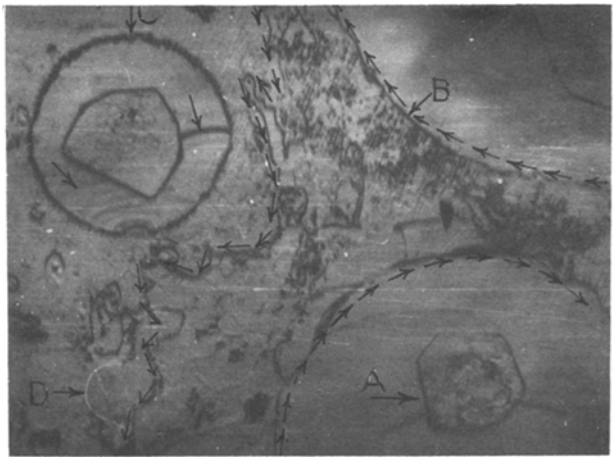

Figure 4 An optical micrograph illustrating several patch-like formations offering evidence of independent growth over them. A is a hexagonal overgrowth, B an irregular and widely spread overgrowth, C a circular overgrowth with a hexagonal overgrowth over it, and D a half microdisc. Note the preferential precipitation of impurities along the edges of B and C and parallel rows of linearly arranged impurity particles on B (× 864).

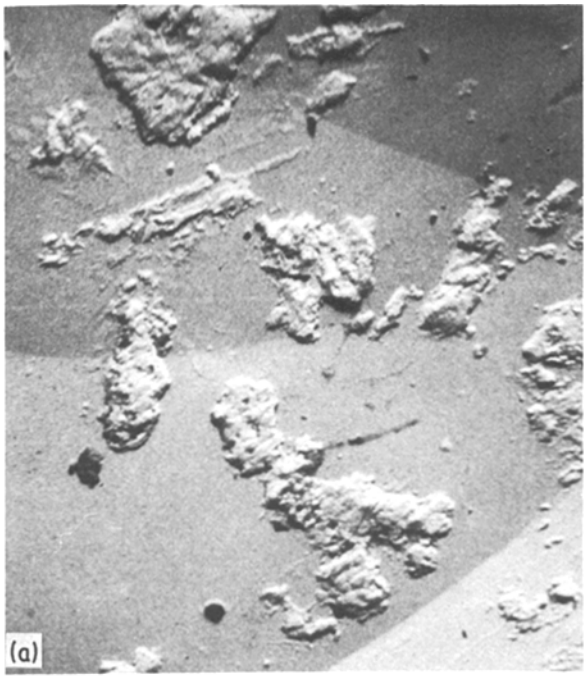

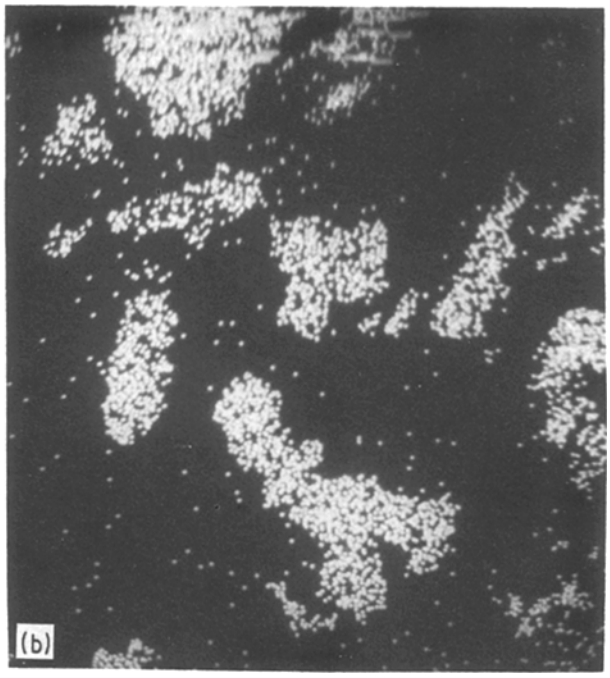

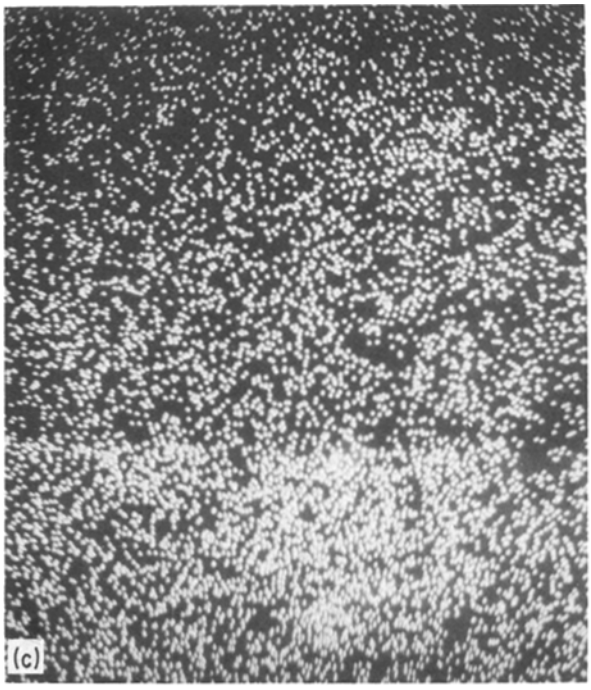

Figure 5 (a) A scanning electron micrograph of lead-rich irregular structures. (b) and (c) EDAX of micrograph shown in (a) detecting (b) Pb$M\alpha$ radiation and thus showing the structure to be rich in lead, and (c) Fe$K\alpha$ radiation thus showing the structures to be rich in iron also ($\times$ 840).

Fig. 5a shows black structures (as observed under the optical microscope) when examined under the SEM. Energy dispersive X-ray analysis (Fig. 5b and c) establishes that the black material (often seen on the crystal surfaces here) corresponds to lead- and iron-rich irregular islands; the energy dispersive X-ray analysis micrographs (b and c) of the region shown in (a) illustrate the detection of Pb$M\alpha$ radiation in (b), confirming the structures to be rich in lead, and the detection of Fe$K\alpha$ radiations in (c), showing the structures to be rich also in iron. It is most probable that the segregated black material in the form of irregular elevations on the surface or as particles along the growth edges (Fig. 1) or at the boundaries of circular or irregular patch-like structures (Figs 2 to 4) is magnetoplumbite. This conclusion receives further support from the literature [9, 10], wherein the authors have established the formation of magnetoplumbite in the case of flux-grown $ErFeO_3$.

On application of EDAX to the patch-like structures, it is established that these structures are highly deficient in iron (there is an almost complete absence of iron). Fig. 6a is the scanning electron micrograph of one of the patch-like structures (giving the appearance of overgrowths). The X-ray mapping of the corresponding region of Fig. 6a shown in Fig. 6b indicates (i) the absence of Fe$K\alpha$ radiation within the region occupied by the overgrowth, showing it to be devoid of iron, and (ii) the detection of Fe$K\alpha$ radiation only on the surface surrounding the irregular structure but not over the irregular structure.

The above observation is further supplemented by the results obtained on other similar irregular structures. Fig. 7 is an electron micrograph of one such irregular structure on the $HoFeO_3$ crystal surface. The horizontal white line across Fig. 7 is the line along which the elemental scan was made. Fig. 8 is the element profile showing registration of Ho$L\alpha$ and Fe$K\alpha$ radiation as we scan from left to right (A–B–C–D). The two traces corresponding to Ho$L\alpha$ and Fe$K\alpha$ radiations have been separated for convenience to avoid confusion due to overlapping. The profile reveals loss of Fe$K\alpha$ radiation and only the continuity of Ho$L\alpha$ radiation in the region B–C indicating thereby a sudden drop in the concentration of iron from the composition of the structure. It thus appears as if the irregular structure were a metal overgrowth of holmium but this is, however, impossible because holmium is far too reactive. The most plausible explanation is that the irregular structure is composed of HoOF which is observed as a secondary

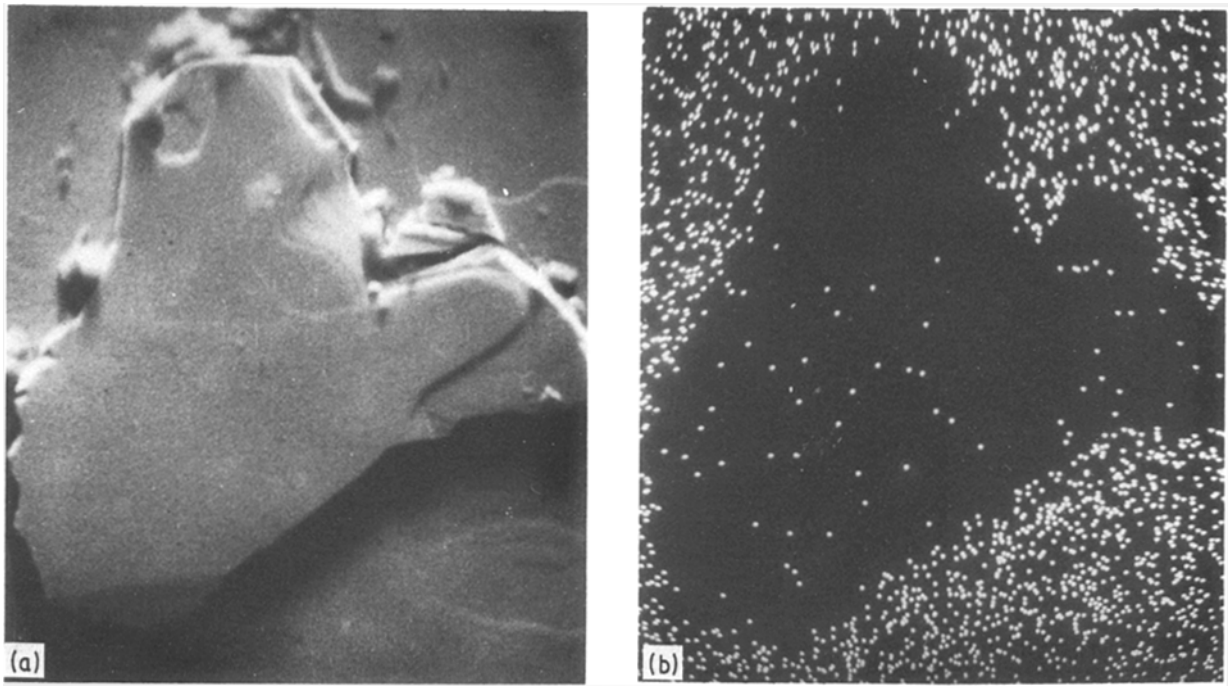

Figure 6 (a) Topograph of crystal surface as seen under the SEM showing an irregular structure observed to be rich in holmium. (b) Energy dispersive X-ray micrograph of the region shown in (a) indicating absence of Fe$K\alpha$ radiation over the surface of the irregular structure, suggesting it to be rich in holmium. Note the detection of Fe$K\alpha$ radiation on the general surface surrounding the irregular structure (× 840).

phase in the flux growth of $HoFeO_3$ under the given growth conditions. The absence of oxygen and fluorine peaks corresponding to the composition HoOF (of the irregular structure) in the profile of Fig. 8 is not surprising since these light elements cannot be detected by this technique.

One might think of the formation of $HoBO_3$ instead of HoOF in view of the starting composition. In order to confirm that the composition is HoOF and not $HoBO_3$, the crystal was subjected to acid (concentrated HNO_3) treatment repeatedly, since $HoBO_3$ is acid soluble. The overgrowths did not show any sign of disappearance, supporting their composition to be HoOF rather than $HoBO_3$.

It is interesting to note that the overgrowths due to precipitation of HoOF developed almost at the end of $HoFeO_3$ crystal growth, as we established by examining the surrounding features of several such overgrowths and finding that there is practically no evidence of modification of $HoFeO_3$ growth fronts by these overgrowths.

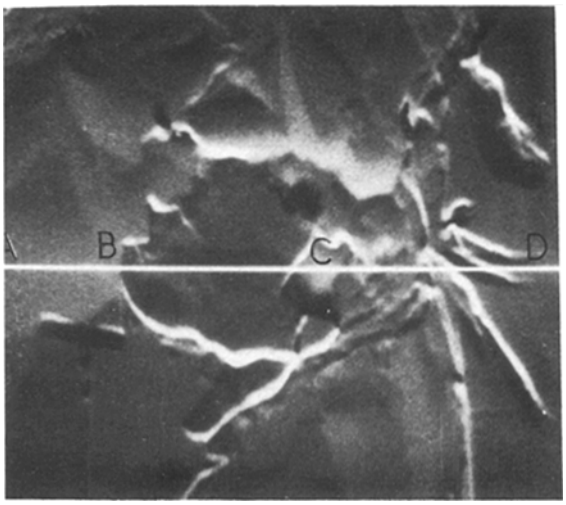

Figure 7 An electron micrograph showing irregular structure on $HoFeO_3$ crystal surface. The horizontal white line A–B–C–D across this figure is the track along which the elemental scan was made (× 2800).

3.3. Microdisc formation

The formation of microdiscs has been attributed to the protective action on the surface by an air bubble during the process of dissolution [11–15] in the case of a wide variety of crystals. Microdisc formation is one of the most frequent observations on flux grown rare-earth orthoferrite crystals. They have been observed in $ErFeO_3$ crystals [10], and $DyFeO_3$ and (HoY) FeO_3 crystals [16]. In the present case, three distinct formations of microdiscs are observed.

The first type seem to have formed at the end of crystal growth. Fig. 9 illustrates a lone microdisc on a reasonably plane surface almost devoid of any other growth structures. Fig. 10 is a microdisc on a surface where thin growth layers are visible. Critical examination indicates continuity of growth layers on either side of the disc. Figs 9 and 10 are examples of microdiscs which formed at the end of growth of $HoFeO_3$ crystals. EDAX studies on the tops of these microdiscs and the general crystal surface outside their periphery indicated major peaks due to holmium, iron and some traces of aluminium and silicon, the analysis expected for $HoFeO_3$. Black spots on the microdisc of Fig. 10 are due to impurities containing lead as the major element which have adhered to the microdisc surface, probably after conditions had become hostile to its further growth.

Traces of aluminium and silicon may be present in the starting materials, but there is no doubt that the major source of aluminium and silicon in the sillimanite

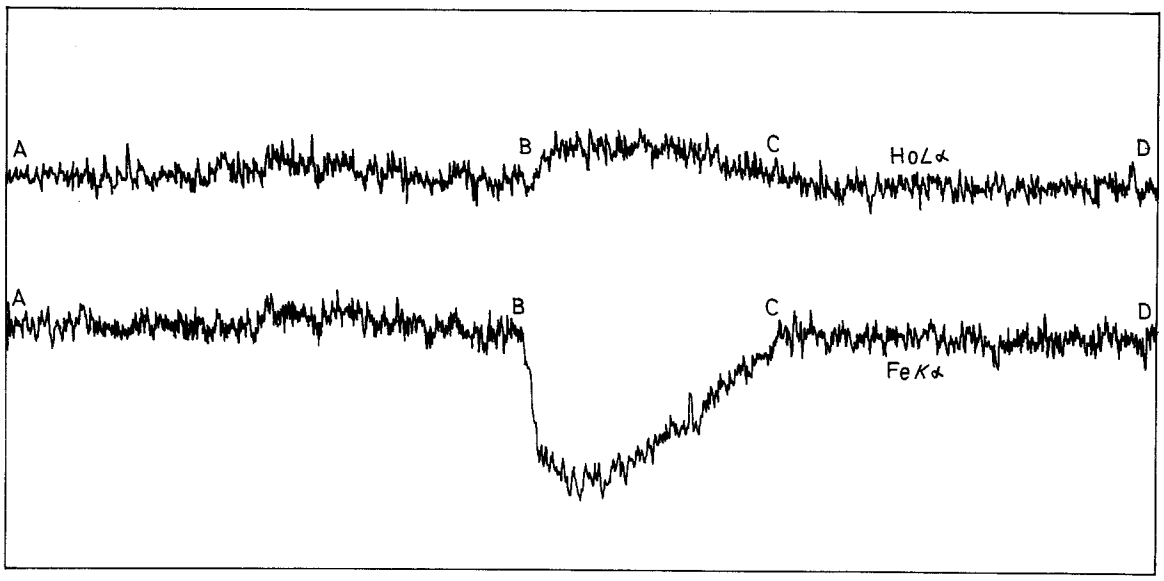

Figure 8 Element profile traced by EDAX showing detection of Ho$L\alpha$ and Fe$K\alpha$ radiation on scanning from left to right. Note loss of Fe$K\alpha$ radiation and the continuity of Ho$L\alpha$ radiation in the region B to C revealing absence of iron from the composition of the irregular structure. (Traces corresponding to Ho$L\alpha$ and Fe$K\alpha$ radiations are separated for convenience.)

(Al_2SiO_5) muffle which contained the crucible in the furnace. Formation of volatile species, capable of transporting aluminium and silicon, is expected at high temperatures by the reaction of PbF_2 with Al_2SiO_5. Thus aluminium and silicon are transported into fluxed melts [17, 18], eventually entering the crystal lattice in substitution for suitable atoms (aluminium substituting for Fe^{3+}).

The second type of microdisc formation is illustrated in Fig. 11. Three microdiscs A, B, C and a fault in the form of an aeroplane wing (D) are seen in the optical micrograph. The fault D is probably a large inclusion (perhaps a microcrystal) which has been partially embedded under the general host crystal surface. Its formation and placement during the continuation of the crystal growth process is clearly evident from the fact that the growth fronts on the general host surface were modified on encountering this obstacle. The growth fronts are clearly seen to have crossed over the fault, which was shifted in this process. The fault has developed strains in the crystal as is evident from cracks clearly visible at its upper boundary. The region containing microdisc A is shown at a higher magnification in Fig. 12. It has a different story to tell. Unlike the microdisc of Figs 9 and 10, this microdisc has obstructed the advancing growth fronts and modified them while they crossed over it and tried to engulf it. Some parts of the microdisc boundary have already disappeared under the growth layers of $HoFeO_3$. The retardation and modification of growth fronts on meeting the already existing microdiscs is abundantly clear. This observation clearly indicates the formation of these microdiscs before crystal growth has ceased (unlike Figs 9 and 10). Had growth continued, the microdiscs would have been completely covered over by the growing surface of the crystal.

The third type of microdisc formation is illustrated in Fig. 13, in which one observes a microdisc and an elevated structure ABC owing to some kind of fault having been embedded into the crystal body by rapidly advancing growth fronts. The modification of growth fronts originating from an active generating centre while wrapping up the fault, is clearly noticed. The microdisc on the broader side A of this fault appears to have been formed much later but before

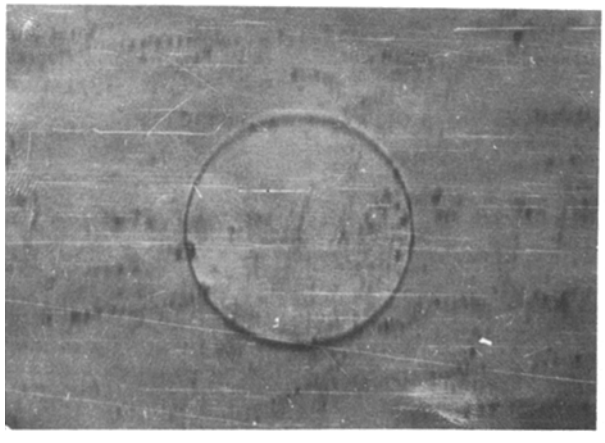

Figure 9 An optical micrograph showing a single microdisc on a surface practically free from any other growth structure (×450).

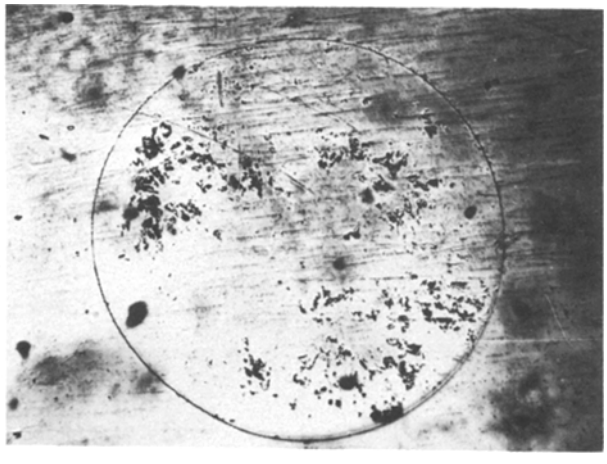

Figure 10 An optical micrograph showing a microdisc with continuity of growth layers on either side of it (×416).

Figure 11 Topograph of a crystal surface as viewed under the optical microscope showing microdiscs A, B, C and a fault D. Notice modification of growth fronts on overriding the fault and cracks on the upper boundary of the fault (× 320).

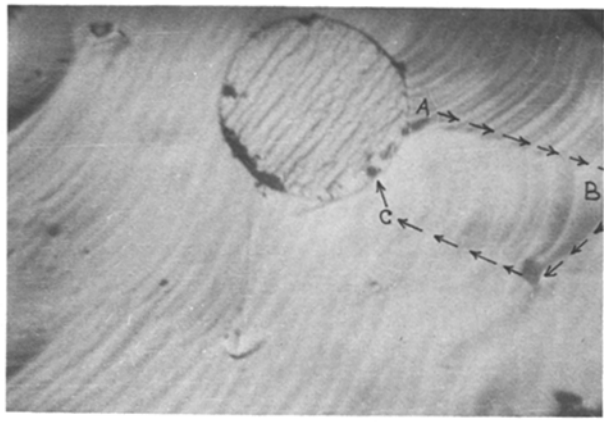

Figure 13 An optical micrograph showing an elevated structure ABC due to burial of a fault by the advancing growth fronts and indicating independent growth on the surface of the adjoining microdisc (× 320).

growth ceased. This inference is drawn because of the indications of independent growth on the surface of the microdisc. Most of the growth layers on the microdisc do not seem to have any connection with the growth fronts on the general surface, though some do give an impression of having crossed over the boundary. The blackness along some parts of the periphery is an impurity rich in lead.

Fig. 14 offers an interesting case of microdiscs in a row oriented in the [0 1 0] direction on a {1 0 0} surface. Features of these microdiscs are that most have a stepped structure, a flat top and are of different sizes both in height as well as in diameter. The black circular structure on the lower extreme of the row (lower left of Fig. 14) is an impurity rich in lead. The two irregular structures, A and B, are elevations which seem to have buried the underlying structure. This is amply clear from the partial coverage of the microdisc on the right-hand side of the irregular structure B. The facet formation of the crystallizing material (of which the overgrowth A and B are composed) is evident. EDAX analysis indicated the irregular structures A and B to have the same composition as those of Fig. 7 which we have suggested is due to precipitation of HoOF after growth has ceased. The surface of the microdisc has the composition $HoFeO_3$ (as indicated by EDAX studies). These observations support the burial of the microdisc structures developed earlier on the surface. The unusual formation of stepped microdiscs is attributed to arhythmic fluctuations in the conditions of crystal growth.

Fig. 15 is an electron micrograph showing two microdiscs A and B and a rounded cavity C. In order to obtain evidence in support of the formation of the microdiscs as being the result of growth of $HoFeO_3$ over impurities, the above micrograph was recorded after indenting one of the microdiscs on the right side (B) so as to chip off a small part of it. The presence of black material (established to be rich in lead and iron by EDAX) under the broken part of the disc supports the view that the formation of these microdiscs can be attributed to the process of $HoFeO_3$ growing over the impurities.

Table I gives a summarized account of the above observations.

4. Conclusions

1. Using the $PbO-PbF_2-B_2O_3$ flux system for the growth of $HoFeO_3$ crystals results in the precipitation

Figure 12 An optical micrograph of the lower middle region at higher magnification revealing the microdisc (A) as an obstruction in the advancement of growth fronts. Notice some parts of the microdisc boundary having disappeared under the growth layers of $HoFeO_3$ (× 1056).

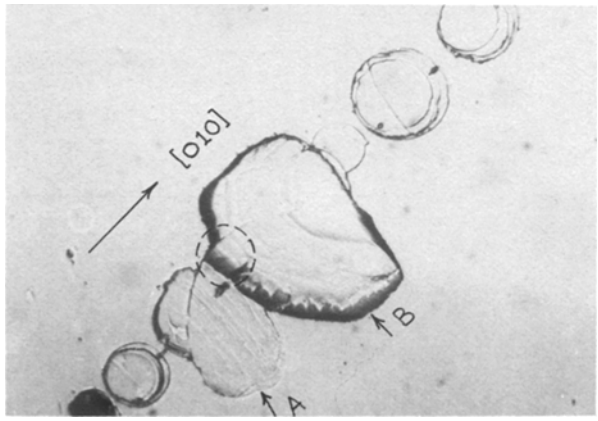

Figure 14 A photomicrograph showing a row of microdiscs oriented in [0 1 0] direction on a {1 0 0} surface. A and B are irregular structures and the facet formation of the crystallizing material due to precipitation of HoOF (× 400).

TABLE I Structures on $HoFeO_3$ crystal surfaces

Structure	Figure	Technique	Analysis	Conclusion	Further note
Main flat surface	Any of the given figures	EDAX	Al and Si present as trace impurities	Al and Si present are transported from Al_2SiO_5 muffle by the reaction of the PbF_2 vapours. Al in the $HoFeO_3$ lattice substitutes for Fe^{3+}	EDAX indicates Al and Si peaks in every case
Wavy growth fronts	1	OM/EDAX	Black material along edges rich in Pb and Fe	Crystallization of impurity phase as magnetoplumbite ($PbO \cdot 6Fe_2O_3$)	Impurities rich in Pb and Fe precipitate preferentially along the edges of the growth fronts
Patch-like structures and scattered particles of black material	2–4	OM/EDAX	Black material rich in Pb and Fe. Traces of Al and Si present	Crystallization of impurity phase as magnetoplumbite ($PbO \cdot 6Fe_2O_3$)	Perfectly circular, semicircular and very irregular patches, some covered by black impurities
Array of particles of black material	2–4	OM/EDAX	Black material rich in Pb and Fe. Traces of Al and Si present	Crystallization of impurity phase as magnetoplumbite ($PbO \cdot 6Fe_2O_3$)	Orderly arrangement along parallel lines in Fig. 4 suggests decoration of defects. Impurity aggregate on left side of Fig. 2 suggested to be defect clusters
Irregular elevations	5a, b, c	SEM/XM	5b shows Pb$M\alpha$ radiation. 5c shows Fe$K\alpha$ radiation. (Features rich in Pb and Fe)	Crystallization of impurity phase as magnetoplumbite ($PbO \cdot 6Fe_2O_3$)	Verified that the black material as seen under OM (Figs 2–4) is rich in Pb and Fe
Irregular overgrowth	6, 7, Structure A and B of Fig. 14	SEM/XM/EPA	Ho present as main component. Fe is absent. The structure did not disappear on acid treatment	Crystallization of secondary phase of composition HoOF likely	Habit formation of secondary phase (HoOF) overgrowths at the end of $HoFeO_3$ crystal growth is seen in Fig. 14
Microdisc pattern	9–15	OM/SEM/EDAX	Exhibit the same peaks in the EDAX curves as the main flat surface of $HoFeO_3$. The black material on the surface (C) of Fig. 15 and under the partially chipped microdisc B is rich in Pb	Formed due to the engulfment by $HoFeO_3$ of impurity phase during growth	Discs mainly of three types: (i) on surface devoid of growth structures or showing continuity of growth fronts on either sides of the disc; (ii) growth fronts crossing over the disc attempting to cover it up, and getting modified in the process; (iii) discs with stepped layers

OM = optical microscopy. SEM = scanning electron microscopy. EDAX = energy dispersive analysis of X-rays. XM = X-ray mapping. EPA = element profile analysis.

of $PbO \cdot 6Fe_2O_3$ (magnetoplumbite) as a secondary phase during growth.

2. HoOF also is precipitated as another secondary phase. This happens mostly at the end of the growth of $HoFeO_3$ crystals.

3. The impurity phases precipitated during growth become enveloped by rapidly advancing growth fronts of $HoFeO_3$ on the growing crystal surface and in this process, result in the formation of microdisc patterns. The microdisc patterns, having the same elemental distribution as the general $HoFeO_3$ crystal surface, were formed on the surface before the cessation of $HoFeO_3$ crystal growth.

4. Aluminium and silicon are present as impurities in all the $HoFeO_3$ crystals studied. These may originate partly from traces of the impurity in the starting composition itself but to a greater extent from the transport of volatile species into the crucible after reaction of volatile PbF_2 with the Al_2SiO_5 furnace muffle. Aluminium no doubt substitutes in the $HoFeO_3$ crystal lattice for Fe^{3+}.

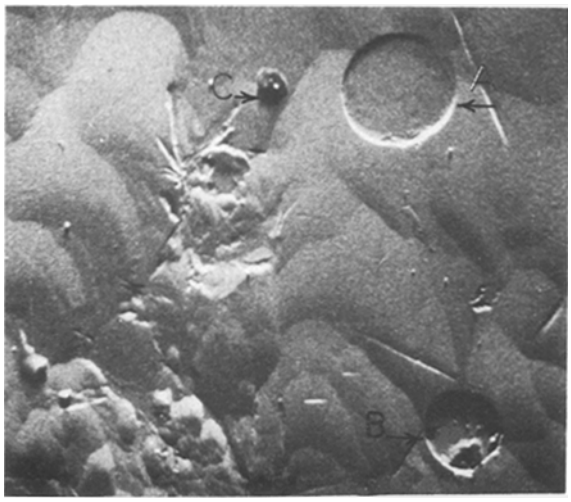

Figure 15 A scanning electron micrograph showing microdiscs A and B and a rounded cavity C. Notice the presence of impurity rich in lead and iron in the form of black material in the indented part of the microdisc B, indicating the formation of the latter due to covering process of the former (× 700).

Acknowledgement

One of us (SKK) is grateful to the University Grants Commission, India, for the award of a Junior Research Fellowship. We thank Dr G. Garton, Head of the Crystal Growth Group, Clarendon Laboratory, University of Oxford, for his encouragement in the collaborative research programme between the Physics Department, University of Jammu, and his Laboratory. The authors also wish to thank Mr V. G. Shah, PRL, Ahmedabad, for his help in the electron microscope work.

References

1. A. V. SHUBNIKOV and N. N. SHEFTAL (eds), "Growth of Crystals", Vol. 1 (Consultants Bureau, New York, 1959).
2. P. N. KOTRU, *Jpn. J. Appl. Phys.* **12** (1973) 790.
3. M. S. JOSHI and P. KOTRU, *Kristall und Tech.* **12** (1977) 13.
4. *Idem, ibid.* **11** (1976) 913.
5. E. D. DUKOVA, *Kristallogr.* **12** (1967) 483 (*Sov. Phys. Crystallogr.* **12** (1967) 413).
6. P. N. KOTRU, S. C. GOSWAMI and B. M. WANKLYN, *J. Mater. Sci.* **18** (1983) 3729.
7. R. M. HORNREICH, *J. Mag. Mag. Mater.* **7** (1978) 280.
8. R. L. WHITE, *J. Appl. Phys.* **40** (1969) 1061.
9. P. N. KOTRU, S. K. KACHROO and B. M. WANKLYN, *J. Mater. Sci. Lett.* **4** (1985) 1273.
10. *Idem, J. Mater. Sci* **21** (1986) 1609.
11. A. A. KUCHARENKO, Monograph on Ural diamonds (exact title not known) (Moscow State Technical Publishing House, 1950).
12. D. C. PANDEYA and S. TOLANSKY, *Proc. Phys. Soc.* **78** (1961) 12.
13. A. R. PATEL and K. N. GOSWAMI, *Proc. Roy. Soc.* **79** (1962) 848.
14. A. R. PATEL and S. TOLANSKY, *ibid.* **A243** (1957) 41.
15. M. S. JOSHI and A. S. VAGH, *Physica* **30** (1964) 1757.
16. P. N. KOTRU, S. K. KACHROO and B. M. WANKLYN, unpublished work.
17. B. M. WANKLYN and Z. HAUPTMAN, *ibid.* **9** (1974) 1078.
18. B. M. WANKLYN and G. GARTON, *ibid.* **9** (1974) 1378.

Received 24 September
and accepted 18 December 1985